

1

2 A proof of concept for neutralizing antibody-guided vaccine design 3 against SARS-CoV-2

4

5

6

7

7 **Author:** Li Zhang^{1\$}, Lei Cao^{2\$}, Xing-Su Gao^{4\$}, Bin-Yang Zheng^{1\$}, Yong-Qiang Deng^{3\$}, Jing-Xin
8 Li^{1,4\$}, Rui Feng², Qian Bian¹, Xi-Ling Guo¹, Nan Wang², Hong-Ying Qiu³, Lei Wang², Zhen Cui²,
9 Qing Ye³, Geng Chen¹, Kui-Kui Lu¹, Yin Chen¹, Yu-Tao Chen², Hong-Xing Pan¹, Bao-Li Zhu¹,
10 Cheng-Feng Qin^{3*}, Xiangxi Wang^{2,5*}, Feng-Cai Zhu^{1,4*}

11

12 Affiliation:

¹³ ¹ National Health Commission of the People's Republic of China, Key laboratory of Enteric
¹⁴ Pathogenic Microbiology (Jiangsu Provincial Center for Disease Control and Prevention), Nanjing
¹⁵ 210009 , China.

² CAS Key Laboratory of Infection and Immunity, National Laboratory of Macromolecules, Institute of Biophysics, Chinese Academy of Sciences, Beijing 100101, China

³ Beijing Institute of Microbiology and Epidemiology, State Key Laboratory of Pathogen and Biosecurity, No. 20 Dongda Street, Fengtai District, Beijing 100071, People's Republic of China.

⁴ Center for Global Health, School of Public Health, Nanjing Medical University, Nanjing 211166, China.

5 Guangzhou Regenerative Medicine and Health Guangdong Laboratory, Guangzhou 510200,
China

24

25

26

27

28

30

30

31 (Email: jszfc@vip.sina.com)

³² These authors contributed equally to this work.

33 **Abstract:** Mutations and transient conformational movements of receptor binding domain (RBD)
34 that make neutralizing epitopes momentarily unavailable, present immune escape routes to
35 SARS-CoV-2. To mitigate viral escape, we developed a cocktail of neutralizing antibodies (Nabs)
36 targeting epitopes located on different domains of spike (S) protein. Screening of a library of
37 monoclonal antibodies generated from peripheral blood mononuclear cells of COVID-19
38 convalescent patients yielded potent Nabs, targeting N-terminal domain (NTD) and RBD domain
39 of S, effective at *nM* concentrations. Remarkably, combination of RBD-targeting Nabs and
40 NTD-binding NAb, FC05, dramatically enhanced the neutralization potency in cell-based assays
41 and animal model. Results of competitive SPR assays and cryo-EM structures of Fabs bound to S
42 unveil determinants of immunogenicity. Combinations of immunogens, identified in NTD and
43 RBD of S, when immunized in rabbits elicited potent protective immune responses against
44 SARS-CoV-2. These results provide a proof-of-concept for neutralization-based immunogen
45 design targeting SARS-CoV-2 NTD and RBD.

46

47 **One sentence summary:**

48 Immunogens identified in the NTD and RBD of the SARS-CoV-2 spike protein using a cocktail of
49 non-competing Nabs when injected in rabbits elicited a potent protective immune response
50 against SARS-CoV-2.

51

52 **Main Text:** Coronavirus disease 2019 (COVID-19), caused by the severe acute respiratory
53 syndrome coronavirus 2 (SARS-CoV-2), continues to spread across the world since December
54 2019 (1, 2). The July 8, 2020 World Health Organization (WHO) Situation Report cited over 11
55 million COVID-19 cases and 539,000 deaths. These numbers continue to rise daily (3).
56 Concerningly, a variant of the SARS-CoV-2 carrying D614G spike mutation, which seemingly
57 enhances the infectivity has been documented and is fast becoming the dominant strain of
58 SARS-CoV-2 globally (4). Safe and effective preventive as well as therapeutic measures are
59 urgently needed to bring the ongoing pandemic of COVID-19 under control (5). Over the past two
60 months, experimental strategies based on eliciting neutralizing antibodies (Nabs) *via*
61 immunization of potential vaccine candidates and passive administration of Nabs have shown
62 promise in protecting and curing SARS-CoV-2-challenged nonhuman primates (6-8). The
63 successes of these studies highlight the importance of screening and identification of immunogens

64 capable of eliciting high NAb titers. Furthermore, NAbs elicited by immunogens differ
65 significantly in their abilities to neutralize SARS-CoV-2 and conferring protection. Therefore, a
66 deep understanding of the nature of NAbs capable of potently neutralizing SARS-CoV-2 and their
67 epitopes could guide new approaches for the development of vaccines.

68

69 The coronavirus spike (S) protein is a multifunctional molecular machine that facilitates viral
70 entry into target cells by engaging with cellular receptors and determines to a great extent cell
71 tropism and host range (9). Coronaviruses S proteins are processed into S1 and S2 subunits by
72 host proteases, among which S1 is responsible for receptor binding, while the S2 subunit mediates
73 membrane fusion (10). The S1 subunit typically possesses two types of domains capable of
74 binding to host cell receptors. For instance, some betacoronaviruses use the N-terminal domain
75 (NTD) of their S1 subunit to bind sialic acids located on the glycosylated cell-surface receptor (11).
76 Similarly, the betacoronavirus murine hepatitis virus uses its NTD for binding the protein receptor
77 CEACAM1 (12). In contrast to this, SARS-CoV and SARS-CoV-2 use the C-terminal domain of
78 their S1 subunit for binding to their protein receptor hACE2 (13). Although it remains unknown
79 whether the NTD is involved in the entry of SARS-CoV-2 into host cells, recent studies have
80 revealed that antibodies targeting the NTD exhibit potent neutralizing activities against
81 SARS-CoV-2 and MERS-CoV infections (14, 15). Abrogation of the crucial role played by the S
82 in the establishment of an infection is the main goal of therapies based on neutralizing antibodies
83 and the focus of antibody-based drug and vaccine design. More recently, a number of
84 RBD-targeting NAbs against SARS-CoV-2, which block the binding of the S trimer to hACE2
85 have been reported and characterized (16-21). Stochastic conformational movements of the RBD
86 transiently expose or hide the determinants of receptor binding and some key neutralizing epitopes,
87 which might open up fortuitous escape routes for the virus. Furthermore, antibody-mediated
88 selective pressure is known to lead to antigenic drift within the RBD, resulting in the accumulation
89 of mutations that hamper neutralization by antibodies (22). To address these issues related to
90 SARS-CoV-2 neutralization, administration of a cocktail of NAbs targeting both the RBD and
91 non-RBD regions, rather than using a single NAb, could potentially increase the potency of
92 protection *via* binding of NAbs to multiple domains of S, thereby preventing escape of the viral
93 particles from the NAbs. In context with this, the immunogenic characteristics of the antigens
94 targeted by potential NAb cocktails and their structural features can inform strategies for the

95 development of vaccines and therapeutics against COVID-19.

96

97 One of the prospective goals of this study was to generate a large and diverse collection of human
98 NAbs targeting multiple domains of S so as to allow for the formulation of a cocktail of highly
99 potent antibodies that could simultaneously bind to the various regions of S. For this, we first
100 established antigen-binding fragment (Fab) phage display libraries from peripheral blood
101 mononuclear cells (PBMCs) of 5 COVID-19 convalescent patients. After three rounds of panning,
102 ~350 randomly picked colonies were screened by enzyme-linked immunosorbent assay (ELISA)
103 for binding to the SARS-CoV-2 S trimer. A set of 202 positive Fab clones exhibiting tight binding
104 to SARS-CoV-2 were selected for sequencing and further analysis (Fig. 1A). We evaluated the
105 ability of these Fabs to bind to recombinant SARS-CoV-2 NTD, RBD or S2 proteins and observed
106 that 40 (~20%), 117 (58%) and 45 (22%) of these monoclonal antibodies (mAbs) recognized the
107 NTD, RBD and S2, respectively (Fig. 1A and 1B). We then narrowed down our selection of
108 candidates for the development of a cocktail to 10 antibodies picked from each of these three
109 groups based on their binding affinities and genetic diversity assessed from the phylogenetic
110 analysis performed using the amino acid sequences of the VHDJH and VLJL regions (23) (Fig. 1A,
111 fig. S1-S2 and Table S1). Among those selected, 3 (named FC01, FC08 and FC11) target the RBD,
112 3 (named FC05, FC06 and FC07) recognize the NTD and 4 (named FC118, FC120, FC122 and
113 FC124) are S2-specific mAbs (Fig. 1C and 1D). To find out whether these antibodies cross-react
114 with SARS-CoV and MERS-CoV, we firstly assessed the binding capacity of these mAbs to RBDs,
115 NTDs and S2s from SARS-CoV-2, SARS-CoV and MERS-CoV by ELISA (Fig. 1C). FC11 and
116 FC07 showed cross-binding to SARS-CoV RBD and NTD, respectively. Expectedly, the four
117 S2-directed mAbs interacted with S2s from all the 3 viruses, of which FC122 bound weakly to
118 SARS-CoV and MERS-CoV (Fig. 1C). Surface plasmon resonance (SPR) assays demonstrated
119 that all 10 mAbs exhibit tight bindings to SARS-CoV-2 with affinities in the range of 0.3-62 nM
120 (Fig. 1D). Interestingly, binding affinities of S2-targeting mAbs were relatively weaker than those
121 of RBD- or NTD-targeting antibodies (Fig. 1D and fig. S3).

122

123 The effectiveness of the neutralization abilities of the 10 mAbs against SARS-CoV-2 infection
124 when tested using Vero-E6 cells revealed that all 10 showed neutralizing activities with IC50
125 values ranging from 0.8-520 nM, among which the 3 RBD-targeting and 1 NTD-binding (FC05)

126 mAbs potently neutralized virus at several nM levels (Fig. 1E). These results, together with the
127 results of the binding site studies, allowed us to rationally evaluate the neutralization potency of
128 the NTD-targeting FC05 in combination with the RBD-targeting NAbs. Not surprisingly, the
129 combination of any one of the RBD-targeting NAbs and FC05 enhanced the neutralization
130 potency dramatically when compared to neutralization performed by using individual NAbs under
131 identical conditions (Fig. 1F). Notably, the cocktail consisting of FC05 (NTD-binding) and FC08
132 (RBD-binding) yielded the strongest neutralizing activity with an IC₅₀ value as low as 15 pM,
133 which was better than the cocktail consisting of FC05 and FC01 as well as other combinations of
134 3 or 4 NAbs (Fig. 1F). Although more recently, synergistic effects between pairs of non-competing
135 RBD-targeting NAbs have been reported for SARS-CoV-2 (19, 22, 24), our cocktail of FC05 and
136 FC08 that bind to different domains of the S trimer provides a proof-of-concept for
137 neutralization-based immunogen design targeting both SARS-CoV-2 NTD and RBD domains.

138

139 Next we sought to assess the *in vivo* protection efficacy of these NAbs against a SARS-CoV-2
140 challenge. A newly established mouse model based on a SARS-CoV-2 mouse adapted strain
141 MASCp6 (25) was used to evaluate potential prophylactic and therapeutic efficacy of these NAbs.
142 BALB/c mice were administered a single dose of 20 mg/kg of FC05 or FC08 or a cocktail of
143 FC05 (NTD-binding) and FC08 (RBD-binding) either 12 h before (day -0.5) or 0.5 day (day 0.5)
144 after viral challenge with 2×10^4 PFU of MASCp6 (BetaCoV/Beijing/IMEBJ05-P6/2020) (Fig.
145 2A). Animals were sacrificed at day 3 for detecting viral loads and examining the pathology of the
146 lungs and tracheas. The number of viral RNA copies estimated in the lungs and tracheas revealed
147 that, in prophylactic settings, a treatment with either individual NAbs or the cocktail led to a 3-4
148 log reduction of viral loads in both lungs and tracheas at day 3 when compared to the PBS-treated
149 group. Notably, a synergistic protective efficacy was observed for the cocktail (Fig. 2B and 2C).
150 The estimated viral loads from the lungs of groups belonging to therapeutic settings showed
151 similar levels as those observed for the groups of the prophylactic settings, however, the viral
152 loads from the tracheas differed for both the groups. An ~10-fold higher titer was observed for the
153 groups in therapeutic settings (Fig. 2B and 2C). Histopathological examination revealed a typical
154 interstitial pneumonia, including widening of alveolar septum, vasodilation, hyperemia and edema,
155 accompanied by a large number of monocytes and lymphocytes and a small number of lobulated
156 granulocytes and other inflammatory cell infiltration in mice belonging to the PBS control group

157 (Fig. 2D). In contrast, no obvious lesions of alveolar epithelial cells or focal hemorrhage were
158 observed in the lung sections from either of the antibody-treated groups at day 3 (Fig. 2D).

159
160 To gain a better understanding of the synergy observed during the neutralization of SARS-CoV-2
161 by a cocktail of NAbs, we performed competitive SPR assays. The results of the assays were
162 expected to reveal whether the NAbs recognize the same or different patches of the epitopes. As
163 expected, the binding of the NTD-specific FC05 does not affect the attachment of any of the three
164 RBD-specific NAbs to the SARS-CoV-2 S trimer, explaining the cooperativity in the antibodies of
165 the cocktail as they bind simultaneously to distinct domains (Fig. 3A). Conversely, the 3
166 RBD-targeting NAbs competed with each other for binding to the SARS-CoV-2 S trimer (Fig. 3B),
167 which may imply that these RBD-targeting antibodies recognize similar epitopes or their epitopes
168 overlap partially. Lastly, none of the 4 S2-specific NAbs were capable of blocking the interactions
169 between soluble hACE2 and the SARS-CoV-2 S trimer (Fig. 3C). To decipher the nature of the
170 epitopes and the mechanism of neutralization at the atomic level, we determined cryo-EM
171 structures of a prefusion stabilized SARS-CoV-2 S ectodomain trimer in complex with the Fab
172 fragments of the NAbs. Surprisingly, the structural studies revealed that all the three
173 RBD-targeting NAbs are capable of destroying the S trimer into monomers or irregular pieces. A
174 similar perturbation of the S trimer was observed previously in the studies conducted on the
175 CR3022 antibody (26). The NTD-binding FC05 however did neither exhibit any such ability of
176 disrupting the S trimer nor did it affect the viral stability (Fig. S4). To gain a deeper understanding
177 of the epitopes targeted by RBD-binding NAbs that disrupt the S trimer, we used a representative
178 antibody, FC08, for performing a competitive SPR-based epitope binding assay. Recently, we
179 mapped the antigenic sites of 3 well characterized RBD-targeting NAbs, H014, HB27 and P17 (16,
180 20, 21), which bind epitopes located on one side of the RBD, the apical head of the RBD and the
181 receptor binding motif (RBM), respectively. Using these previously characterized antibodies along
182 with FC08 in the assays revealed that only P17 competes with FC08 for binding to the
183 SARS-CoV-2 S trimer. H014 and HB27, as well as the hACE2 can simultaneously bind to
184 SARS-CoV-2 S trimer together with FC08 (Fig. 3D-3F). This observation coupled with an ability
185 of dispersing the S trimer into monomers, suggests that FC08 probably recognizes a cryptic
186 epitope lying towards the interior of the S trimer (Fig. 3D-3F). Cryo-EM characterization of the
187 S-FC05 complex showed full occupancy where one Fab is bound to each NTD of the

188 homotrimeric S (Fig. 3G). 3D classification revealed that the S trimer adopts a 3-fold symmetrical
189 structure with all three RBDs closed albeit without imposing any symmetry. By applying a C3
190 symmetry, we reconstructed the cryo-EM structure of the complex at an overall resolution of 3.4
191 Å. A “block-based” reconstruction approach was used to improve the local resolution (3.9 Å) of
192 the map around the binding interface between NTD and FC05 (Fig. 3G, fig. S5-S7 and table S2).
193 Interestingly, the binding mode of FC05 resembles with that of 4A8, a recently reported
194 SARS-CoV-2 NAb (14) (fig. S8). Similar to 4A8, FC05 recognizes a conformational epitope
195 formed by elements of the N3 and N5 loops located on the NTD with a buried surface area of
196 ~700 Å². The essential epitope contains 12 residues, among which all 12 residues (100 %) are not
197 conserved between SARS-CoV and SARS-CoV-2, explaining FC05’s virus-specific binding and
198 neutralization activities (Fig. 3H-3I and fig. S9). The paratope of FC05 is composed of 4
199 complementarity-determining regions (CDR) loops: CDRL2 (residues 49-55), CDRH1 (residues
200 29-33), CDRH2 (residues 50-59) and CDRH3 (residues 99-106) (table S3). Extensive
201 hydrophobic and hydrophilic interactions facilitate the tight binding between FC05 and the NTD.
202 Analysis of the structures also provides structural basis for rationalizing the cooperativity
203 observed when both FC05 and FC08 are used for neutralizing SARS-CoV-2.

204

205 Most of the potent neutralizing antibodies reported till date target the RBD of CoV (18-20).
206 Therefore, a number of RBD-subunit based vaccines for protection against SARS, MERS and
207 COVID-19 are under development (27-29). However, RBD-subunit based vaccines could face
208 some critical challenges arising from their relatively low immunogenicity, less diversity within the
209 elicited antibodies and the ensuing potential escape of viral mutants from the antibodies under
210 selective pressure. Our study here, together with other recently published studies, indicates that a
211 subset of NTD-directed antibodies possesses potent neutralizing activities (Fig. 1 and Fig. 2) and
212 that cocktails of antibodies containing NTD-directed as well as RBD-targeting NAb act in
213 synergy to confer protection against SARS-CoV-2, suggestive of the NTD to be a promising
214 immunogenic partner of the SARS-CoV-2 RBD. To verify this idea, 16 groups of New Zealand
215 rabbits (n=4/group) were injected at day 0, 14 and 28 with various doses of candidate antigen
216 formulations mixed with alum or AS01B adjuvant as follows - 5 µg RBD or 5 µg NTD or 2.5 µg
217 RBD + 2.5 µg NTD; or 20 µg RBD or 20 µg RBD or 10 µg RBD + 10 µg NTD; or 20 µg RBD +
218 20 µg NTD per dose, 0 µg of antigens in physiological saline as the sham group (Fig. 4). No

219 inflammation or other adverse effects were observed in the animals. Titers of
220 SARS-CoV-2-specific neutralizing antibodies produced by the animals over a period of time (at
221 week 0, 2, 4 and 6) effective in neutralizing the live virus were monitored using
222 microneutralization assays (MN50). Similar to the immune responses elicited by an inactivated
223 SARS-CoV2 vaccine candidate (PiCoVacc) reported by us previously, the neutralizing antibody
224 titer emerged at week 2, surged at week 4 and continued to increase at week 6 (Fig. 4). Perhaps
225 correlated with the less glycosylation and more neutralizing epitopes present in RBD, the RBD
226 induced much higher NAb titers than the NTD at various doses. However, the combination of
227 RBD and NTD exhibited more robust and stable immunogenicity for neutralization compared with
228 a single immunogen consisting of either RBD or NTD at the same dose tested under identical
229 conditions (Fig. 4). Notably, relatively large differences in the ability of individual animals in
230 eliciting NAb titers were observed within the RBD vaccinated groups. Addition of NTD to RBD
231 not only substantially enhanced the NAb titer, but also remarkably decreased the fluctuation in
232 eliciting NAb titer from immunized animals (Fig. 4). Compared to AS01B, alum based adjuvant
233 facilitates the antigens in boosting immune responses at 5 or 20 µg/dose. Administration of higher
234 doses of antigens during immunization (20 µg RBD + 20 µg NTD) with AS01B led to the highest
235 NAb titer, up to ~1000. In contrast, immunization with higher doses of antigens in conjunction
236 with alum yielded a decreased NAb titer (~200) compared to the median dose (10 µg RBD + 10
237 µg NTD), indicative of the need for proper collocation of the adjuvant and various doses of
238 antigen during immunization (Fig. 4).

239
240 COVID-19 vaccine development is moving at unprecedented speed, with more than 250
241 candidates under development worldwide. Except for a few inactivated SARS-CoV-2 virus
242 vaccines, most of the candidate vaccines are aimed at the RBD or the spike of SARS-CoV-2 as
243 target immunogen. Selection of the target immunogen is critical for the success of a vaccine, since
244 eliciting a large amount of antibody that binds, but does not neutralize, may lead to low protection
245 or even immunopathology (30). The ideal immunogen should elicit high-quality, functionally
246 neutralizing antibodies while avoiding induction of non-neutralizing antibodies. We are now
247 entering a new era of precision vaccinology in which multi-disciplinary techniques provide
248 avenues to rapidly isolate and characterize human NAb, to define the structural basis of
249 antigenicity, to understand mechanisms of viral neutralization and to guide rational immunogen

250 design. The immunogenic data derived from immunization with a combination of SARS-CoV-2
251 RBD and NTD here demonstrates the feasibility of eliciting robust targeted immune profiles by
252 using antibody-guided vaccine design and advance us a step forward towards a future of precision
253 vaccines.

254

255

256 **References and Notes**

- 257 1. N. Zhu, D. Zhang *et al.*, A Novel Coronavirus from Patients with Pneumonia in China, 2019.
258 *The New England journal of medicine* **382**, 727-733 (2020); published online EpubFeb 20
259 (10.1056/NEJMoa2001017).
- 260 2. N. Chen, M. Zhou *et al.*, Epidemiological and clinical characteristics of 99 cases of 2019 novel
261 coronavirus pneumonia in Wuhan, China: a descriptive study. *Lancet (London, England)* **395**,
262 507-513 (2020); published online EpubFeb 15 (10.1016/s0140-6736(20)30211-7).
- 263 3. W. H. Organization. (July 8, 2020).
- 264 4. B. Korber, W. M. Fischer *et al.*, Tracking changes in SARS-CoV-2 Spike: evidence that D614G
265 increases infectivity of the COVID-19 virus. *Cell*, (2020); published online Epub2020/07/03/
266 (https://doi.org/10.1016/j.cell.2020.06.043).
- 267 5. K. P. O'Callaghan, A. M. Blatz *et al.*, Developing a SARS-CoV-2 Vaccine at Warp Speed. *Jama*,
268 (2020); published online EpubJul 6 (10.1001/jama.2020.12190).
- 269 6. Q. Gao, L. Bao *et al.*, Rapid development of an inactivated vaccine candidate for SARS-CoV-2.
270 *Science*, (2020); published online EpubMay 6 (10.1126/science.abc1932).
- 271 7. J. Yu, L. H. Tostanoski *et al.*, DNA vaccine protection against SARS-CoV-2 in rhesus macaques.
272 *Science*, (2020); published online EpubMay 20 (10.1126/science.abc6284).
- 273 8. R. Shi, C. Shan *et al.*, A human neutralizing antibody targets the receptor-binding site of
274 SARS-CoV-2. *Nature*, (2020); published online EpubMay 26 (10.1038/s41586-020-2381-y).
- 275 9. F. Li, Structure, Function, and Evolution of Coronavirus Spike Proteins. *Annual review of
276 virology* **3**, 237-261 (2016); published online EpubSep 29
277 (10.1146/annurev-virology-110615-042301).
- 278 10. M. Hoffmann, H. Kleine-Weber *et al.*, SARS-CoV-2 Cell Entry Depends on ACE2 and TMPRSS2
279 and Is Blocked by a Clinically Proven Protease Inhibitor. *Cell* **181**, 271-280 e278 (2020);
280 published online EpubApr 16 (10.1016/j.cell.2020.02.052).
- 281 11. X. Huang, W. Dong *et al.*, Human Coronavirus HKU1 Spike Protein Uses O-Acetylated Sialic
282 Acid as an Attachment Receptor Determinant and Employs Hemagglutinin-Esterase Protein as
283 a Receptor-Destroying Enzyme. *Journal of virology* **89**, 7202-7213 (2015); published online
284 EpubJul (10.1128/JVI.00854-15).
- 285 12. J. Shang, Y. Wan *et al.*, Structure of mouse coronavirus spike protein complexed with receptor
286 reveals mechanism for viral entry. *PLoS pathogens* **16**, e1008392 (2020); published online
287 EpubMar (10.1371/journal.ppat.1008392).
- 288 13. J. Shang, Y. Wan *et al.*, Cell entry mechanisms of SARS-CoV-2. *Proceedings of the National
289 Academy of Sciences of the United States of America* **117**, 11727-11734 (2020); published
290 online EpubMay 26 (10.1073/pnas.2003138117).

291 14. X. Chi, R. Yan *et al.*, A neutralizing human antibody binds to the N-terminal domain of the
292 Spike protein of SARS-CoV-2. *Science*, (2020); published online EpubJun 22
293 (10.1126/science.abc6952).

294 15. H. Zhou, Y. Chen *et al.*, Structural definition of a neutralization epitope on the N-terminal
295 domain of MERS-CoV spike glycoprotein. *Nature communications* **10**, 3068 (2019); published
296 online EpubJul 11 (10.1038/s41467-019-10897-4).

297 16. Y.-Q. D. Zhe Lv, Qing Ye, Lei Cao, Chun-Yun Sun, Changfa Fan, Weijin Huang, Shihui Sun, Yao
298 Sun, Ling Zhu, Qi Chen, Nan Wang, Jianhui Nie, Zhen Cui, Dandan Zhu, Neil Shaw, Xiao-Feng Li,
299 Qianqian Li, Liangzhi Xie, Youchun Wang, Zihe Rao, Cheng-Feng Qin, Xiangxi Wang, Structural
300 basis for neutralization of SARS-CoV-2 and SARS-CoV by a potent therapeutic antibody.
301 *bioRxiv : the preprint server for biology*, (2020).

302 17. D. Pinto, Y. J. Park *et al.*, Cross-neutralization of SARS-CoV-2 by a human monoclonal
303 SARS-CoV antibody. *Nature* **583**, 290-295 (2020); published online EpubJul
304 (10.1038/s41586-020-2349-y).

305 18. A. Z. Wec, D. Wrapp *et al.*, Broad neutralization of SARS-related viruses by human monoclonal
306 antibodies. *Science*, (2020); published online EpubJun 15 (10.1126/science.abc7424).

307 19. P. J. M. Brouwer, T. G. Caniels *et al.*, Potent neutralizing antibodies from COVID-19 patients
308 define multiple targets of vulnerability. *Science*, (2020); published online EpubJun 15
309 (10.1126/science.abc5902).

310 20. Y.-Q. D. Ling Zhu, Rong-Rong Zhang, Zhen Cui, Chun-Yun Sun, Chang-Fa Fan, Liangzhi Xie,
311 Youchun Wang, Xiangxi Wang, Cheng-Feng Qin, Double Lock of a Potent Human Therapeutic
312 Monoclonal Antibody against SARS-CoV-2. *bioRxiv : the preprint server for biology*, (2020).

313 21. Y. S. Hangping Yao, Yong-Qiang Deng, Nan Wang, Xiao-Feng Li, Yongcong Tan, Na-na Zhang,
314 Luanjuan Li, Cheng-Feng Qin, Xiangxi Wang, Rational Development of a Human Antibody
315 Cocktail that Deploys Multiple Functions to Confer Pan-SARS-CoVs Protection. *bioRxiv : the
316 preprint server for biology*, (2020).

317 22. A. Baum, B. O. Fulton *et al.*, Antibody cocktail to SARS-CoV-2 spike protein prevents rapid
318 mutational escape seen with individual antibodies. *Science*, (2020); published online
319 EpubJun 15 (10.1126/science.abd0831).

320 23. S. Kumar, G. Stecher *et al.*, MEGA7: Molecular Evolutionary Genetics Analysis Version 7.0 for
321 Bigger Datasets. *Molecular biology and evolution* **33**, 1870-1874 (2016); published online
322 EpubJul (10.1093/molbev/msw054).

323 24. Y. Wu, F. Wang *et al.*, A noncompeting pair of human neutralizing antibodies block COVID-19
324 virus binding to its receptor ACE2. *Science* **368**, 1274-1278 (2020); published online EpubJun
325 12 (10.1126/science.abc2241).

326 25. H. Gu, Q. Chen *et al.*, Rapid adaptation of SARS-CoV-2 in BALB/c mice: Novel mouse model for
327 vaccine efficacy. *bioRxiv*, 2020.2005.2002.073411 (2020)10.1101/2020.05.02.073411).

328 26. J. Huo, Y. Zhao *et al.*, Neutralization of SARS-CoV-2 by Destruction of the Prefusion Spike. *Cell
329 host & microbe*, (2020); published online EpubJun 19 (10.1016/j.chom.2020.06.010).

330 27. L. Dai, T. Zheng *et al.*, A Universal Design of Betacoronavirus Vaccines against COVID-19,
331 MERS, and SARS. *Cell*, (2020); published online EpubJun 28 (10.1016/j.cell.2020.06.035).

332 28. N. Wang, J. Shang *et al.*, Subunit Vaccines Against Emerging Pathogenic Human Coronaviruses.
333 *Frontiers in microbiology* **11**, 298 (2020)10.3389/fmicb.2020.00298).

334 29. J. Yang, W. Wang *et al.*, A vaccine targeting the RBD of the S protein of SARS-CoV-2 induces

335 protective immunity. *Nature*, (2020); published online EpubJul 29
336 (10.1038/s41586-020-2599-8).

337 30. B. S. Graham, Rapid COVID-19 vaccine development. *Science (New York, N.Y.)* **368**, 945-946
338 (2020); published online EpubMay 29 (10.1126/science.abb8923).

339 31. C. F. Barbas, 3rd, A. S. Kang *et al.*, Assembly of combinatorial antibody libraries on phage
340 surfaces: the gene III site. *Proceedings of the National Academy of Sciences of the United
341 States of America* **88**, 7978-7982 (1991); published online EpubSep 15
342 (10.1073/pnas.88.18.7978).

343 32. Z. Chen, X. Ren *et al.*, An elaborate landscape of the human antibody repertoire against
344 enterovirus 71 infection is revealed by phage display screening and deep sequencing. *mAbs* **9**,
345 342-349 (2017); published online EpubFeb/Mar (10.1080/19420862.2016.1267086).

346 33. D. N. Mastronarde, Automated electron microscope tomography using robust prediction of
347 specimen movements. *Journal of structural biology* **152**, 36-51 (2005); published online
348 EpubOct (10.1016/j.jsb.2005.07.007).

349 34. K. Zhang, Gctf: Real-time CTF determination and correction. *Journal of structural biology* **193**,
350 1-12 (2016); published online EpubJan (10.1016/j.jsb.2015.11.003).

351 35. S. H. Scheres, Processing of Structurally Heterogeneous Cryo-EM Data in RELION. *Methods in
352 enzymology* **579**, 125-157 (2016)10.1016/bs.mie.2016.04.012).

353 36. S. H. Scheres, S. Chen, Prevention of overfitting in cryo-EM structure determination. *Nature
354 methods* **9**, 853-854 (2012).

355 37. Y. Yang, P. Yang *et al.*, Architecture of the herpesvirus genome-packaging complex and
356 implications for DNA translocation. *Protein & cell* **11**, 339-351 (2020); published online
357 EpubMay (10.1007/s13238-020-00710-0).

358 38. N. Wang, D. Zhao *et al.*, Architecture of African swine fever virus and implications for viral
359 assembly. *Science* **366**, 640-644 (2019); published online EpubNov 1
360 (10.1126/science.aaz1439).

361 39. N. Wang, W. Chen *et al.*, Structures of the portal vertex reveal essential protein-protein
362 interactions for Herpesvirus assembly and maturation. *Protein & cell* **11**, 366-373 (2020);
363 published online EpubMay (10.1007/s13238-020-00711-z).

364 40. A. Kucukelbir, F. J. Sigworth *et al.*, Quantifying the local resolution of cryo-EM density maps.
365 *Nature methods* **11**, 63-65 (2014).

366 41. L. A. Kelley, S. Mezulis *et al.*, The Phyre2 web portal for protein modeling, prediction and
367 analysis. *Nature Protocols* **10**, 845-858 (2015); published online EpubJun
368 (10.1038/nprot.2015.053).

369 42. E. F. Pettersen, T. D. Goddard *et al.*, UCSF Chimera—a visualization system for exploratory
370 research and analysis. *Journal of computational chemistry* **25**, 1605-1612 (2004).

371 43. A. Brown, F. Long *et al.*, Tools for macromolecular model building and refinement into
372 electron cryo-microscopy reconstructions. *Acta Crystallographica Section D-Structural Biology*
373 **71**, 136-153 (2015); published online EpubJan (10.1107/S1399004714021683).

374 44. P. V. Afonine, R. W. Grosse-Kunstleve *et al.*, Towards automated crystallographic structure
375 refinement with phenix. refine. *Acta Crystallographica Section D: Biological Crystallography*
376 **68**, 352-367 (2012).

377 45. V. B. Chen, W. B. Arendall *et al.*, MolProbity: all-atom structure validation for macromolecular
378 crystallography. *Acta Crystallographica Section D: Biological Crystallography* **66**, 12-21 (2010).

379 46. P. Gouet, E. Courcelle *et al.*, ESPript: analysis of multiple sequence alignments in PostScript.
380 *Bioinformatics* **15**, 305-308 (1999).
381

382 **Acknowledgments:** We thank Prof. Zihe Rao for valuable discussion on this project and thank
383 Drs. Chunyun Sun, and Changfa Fan for providing critical reagents and thank Drs. Xiaojun Huang,
384 Boling Zhu and Gang Ji for cryo-EM data collection, the Center for Biological imaging (CBI) in
385 Institute of Biophysics for EM work. This work was supported by the National Key Research and
386 Development Program (2020YFA0707500, 2018YFA0900801), the Strategic Priority Research
387 Program (XDB29010000), National Natural Science Foundation of China (NSFC) (grants
388 82041005, 31900873). Feng-Cai Zhu and Li Zhang were supported by the Research and
389 development project of Jiangsu Province (BE20200601) and The Social Development Project of
390 Jiangsu Province (BE2020720). Xiangxi Wang was supported by Ten Thousand Talent Program
391 and the NSFS Innovative Research Group (No. 81921005). Cheng-Feng Qin was supported by the
392 National Science Fund for Distinguished Young Scholar (No. 81925025) and the Innovative
393 Research Group (No. 81621005) from the NSFC, and the Innovation Fund for Medical Sciences
394 (No.2019-I2M-5-049) from the Chinese Academy of Medical Sciences.

395 **Author contribution:** F-C.Z., X.W. and C-F.Q conceived, designed and supervised the study and
396 wrote the paper. L.Z., X-S.G., B-Y.Z., contributed in construction of the antibody libraries,
397 panning and sequencing of mAbs, generation of mAbs, and the cross-reaction of mAbs. J-X.L.
398 contributed in the paper drafting, plotting histogram, and data interpretation. H-X.P., B-L.Z.
399 collected data. X-L.G., Y.C., performed neutralizing activities assay (CPE) in Vero-E6 cells. Q.B.,
400 G.C., K-K. L., evaluated safety and immunogenicity of a recombinant two components candidate
401 COVID-19 vaccine in New Zealand rabbits. C.L. purified proteins, prepared cryo-EM grids and
402 collected cryo-EM data. Y-Q.D. and Q.Y. performed live virus and animal assays; N.W., L.W., L.C.
403 and X.W. processed data. L.C. built and refined the structure model. N.W., L.C. and X.W.
404 analyzed the structures. R.F. performed SPR assay. All authors read and approved the contents of
405 the manuscript.

406 **Data and materials availability:** Cryo-EM density maps have been deposited at the Electron
407 Microscopy Data Bank with accession codes EMD-XXXX (SARS-CoV-2 S-FC05) and
408 EMD-YYYY (SARS-CoV-2 S in complex with FC05 and H014) and related atomic models have
409 been deposited in the protein data bank under accession code 6XXX and 6YYY, respectively.

410

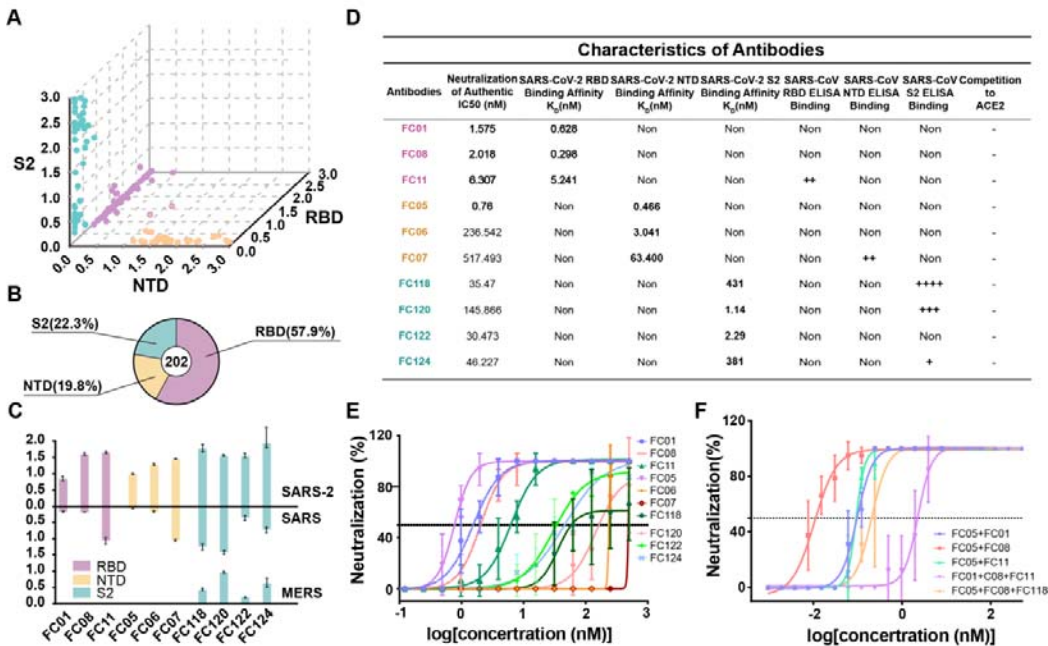


Figure 1. Identification and characterization of SARS-CoV-2 S-targeting neutralizing antibodies. (A) Characteristics of antibodies binding to SARS-CoV-2 RBD, NTD or S2 by ELISA. SARS-CoV-2 RBD-, NTD- and S2-specific mAbs are colored in pink, wheat and pale cyan dots, respectively. A number of mAbs that exhibit non-specific bindings to both SARS-CoV-2 RBD and NTD are presented in wheat dots with pink outlines. (B) Proportion of SARS-CoV-2 S-specific antibodies targeting each of the indicated domains. (C) Bar graph depicting the binding of 10 representative mAbs (FC01, FC05, FC06, FC07, FC08, FC11, FC118, FC120, FC122 and FC124) to S proteins of SARS-CoV-2, SARS-CoV and MERS-CoV using ELISA assays (shown as mean \pm S.D. of values derived from experiments conducted in triplicate). (D) Summary of the performance of the representative 10 mAbs in the indicated assays. *In vitro* neutralization activities of 10 individual mAbs (E) or the cocktail of antibodies (F) against SARS-CoV-2 in Vero-E6 cells. Neutralizing activities are represented as mean \pm SD. Experiments were performed in triplicates

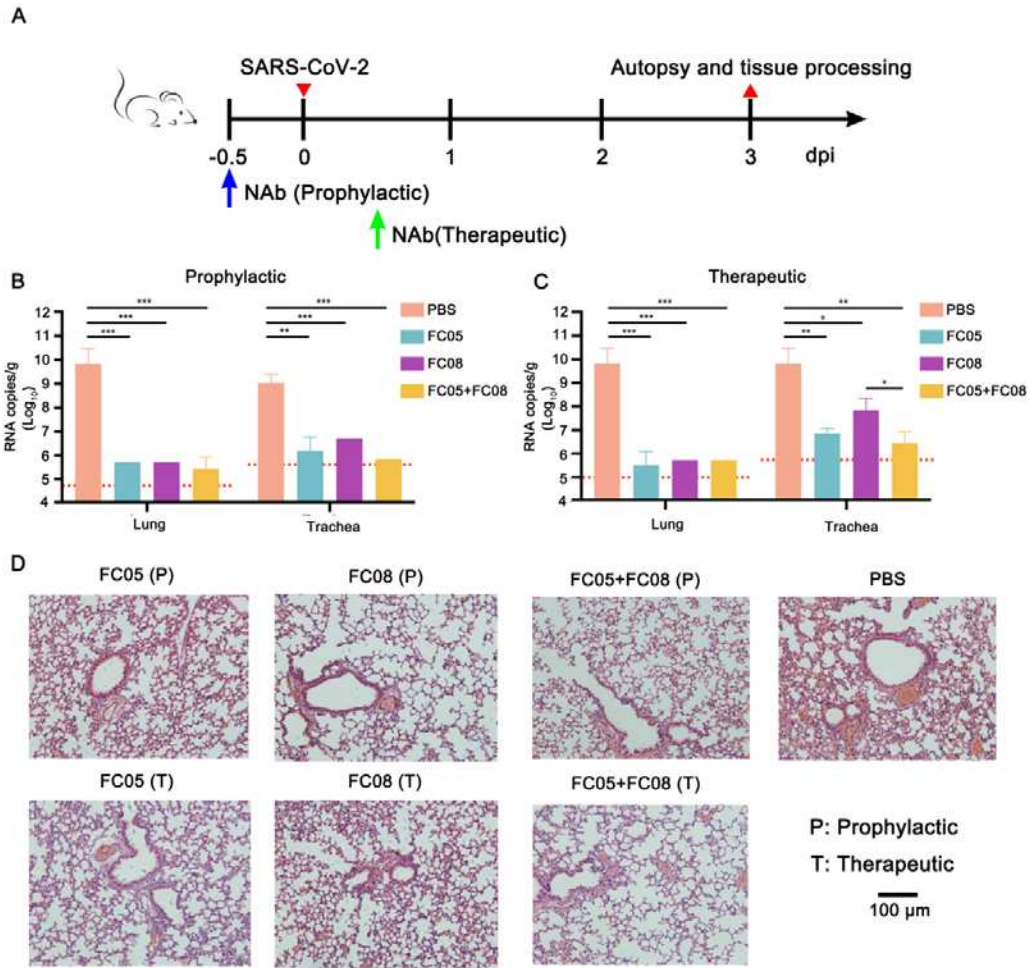
425

426

427

428

429



430 **Figure 2 Prophylactic and therapeutic efficacy of FC05 or FC08 or the cocktail of antibodies**
431 **of FC05 and FC08 in SARS-CoV-2 susceptible mice model.** (A) Experimental design for
432 therapeutic and prophylactic evaluations of FC05 or FC08 or the cocktail of antibodies consisting
433 of FC05 and FC08 by using a mouse adapted SARS-CoV-2 virus (MASCp6) in mice model.
434 Group of BALB/c mice were infected intranasally with 2×10^4 PFU of MASCp6. A dose of 20
435 mg/kg of antibody was administrated intraperitoneally at 12 hours before infection (the
436 prophylactic group, P) or at 2 hours after infection (the therapeutic group, T). PBS injection was
437 used as a negative control group. Then, the lung and the trachea tissues of mice were collected at 3
438 and 5 dpi for virus load measurement and histopathological analysis. (B) and (C) Virus loads of
439 lung and trachea tissues at 3 dpi in mouse model. The viral loads of the tissues were determined
440 by qRT-PCR (*P<0.05; **P<0.01; ***P<0.001). Data are represented as mean \pm SD. Dashed lines

441 represent the limit of detection. (D) Histopathological analysis of lung and trachea samples at 3
442 dpi. Scale bar: 100 μ m.

443

444

445

446

447

448

449

450

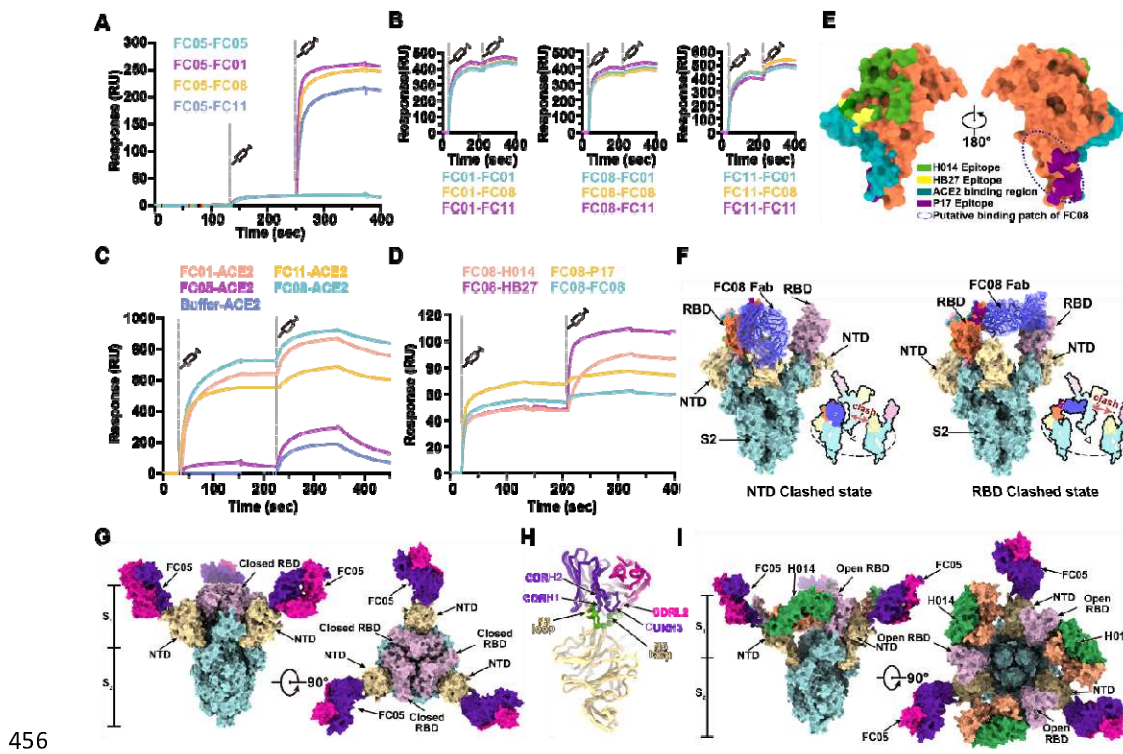
451

452

453

454

455



456

457 **Figure 3. Epitope mapping of SARS-CoV-2 NAbs.** (A) SPR kinetics of simultaneous binding of
458 FC05 and 3 RBD-directed NAbs to SARS-CoV-2 S trimer. (B) SPR-based competitive binding of
459 3 RBD-directed NAbs to SARS-CoV-2 S trimer. SARS-CoV-2 S trimer was initially immobilized
460 onto the sensor. 1 NAb was first injected, followed by the other 2, which indicated these 3
461 RBD-directed NAbs competed with each other for binding to the SARS-CoV-2 S trimer. (C)
462 Binding of any one RBD-directed NAb blocks the interactions between ACE2 and SARS-CoV-2
463 S trimer assessed by competitive SPR. (D) Competitive SPR-based epitope mapping of FC08
464 through 3 recently well characterized RBD-targeting SARS-CoV-2 NAbs, H014, HB27 and P17.
465 The results indicate P17 competes with FC08 for binding to the SARS-CoV-2 S trimer, while
466 H014 and HB27 are capable of simultaneously binding to SARS-CoV-2 S trimer together with
467 FC08. (E) FC08 epitope analysis on the RBD surface. The epitope clusters of H014, P17 and
468 HB27, and the binding region for ACE2 are shown in indicated colors. Putative epitopes are
469 indicated by dashed lines. (F) Two putative models for FC08 binding to SARS-CoV-2 S trimer.
470 Domains of S2 and NTD are colored in cyan and yellow, respectively. The color scheme for the
471 RBD bound FC08 is same as Fig. 3E and the other 2 RBDs are colored in violet. FC08 Fab is
472 presented as blue cartoon with 50% transparent surface. (G) Cryo-EM structure of SARS-CoV-2 S
473 trimer-FC05 complex. Each S monomer is depicted by various colors and the FC05 Fabs are

474 shown in hotpink (light chains) and purpleblue (heavy chains). (H) Interactions between the NTD
475 and FC05. The loops involved in interactions with FC05 are highlighted in green and key CDRs
476 are labeled. (I) Surface representation of the RBD of SARS-CoV-2 S. The areas buried
477 by FC05 is marked by sky blue lines. Sequence identities and differences between the
478 S of SARS-CoV and SARS-CoV-2 are shown in pink and green, respectively,
479 mapped on the surface of SARS-CoV-2 S/RBD.

480

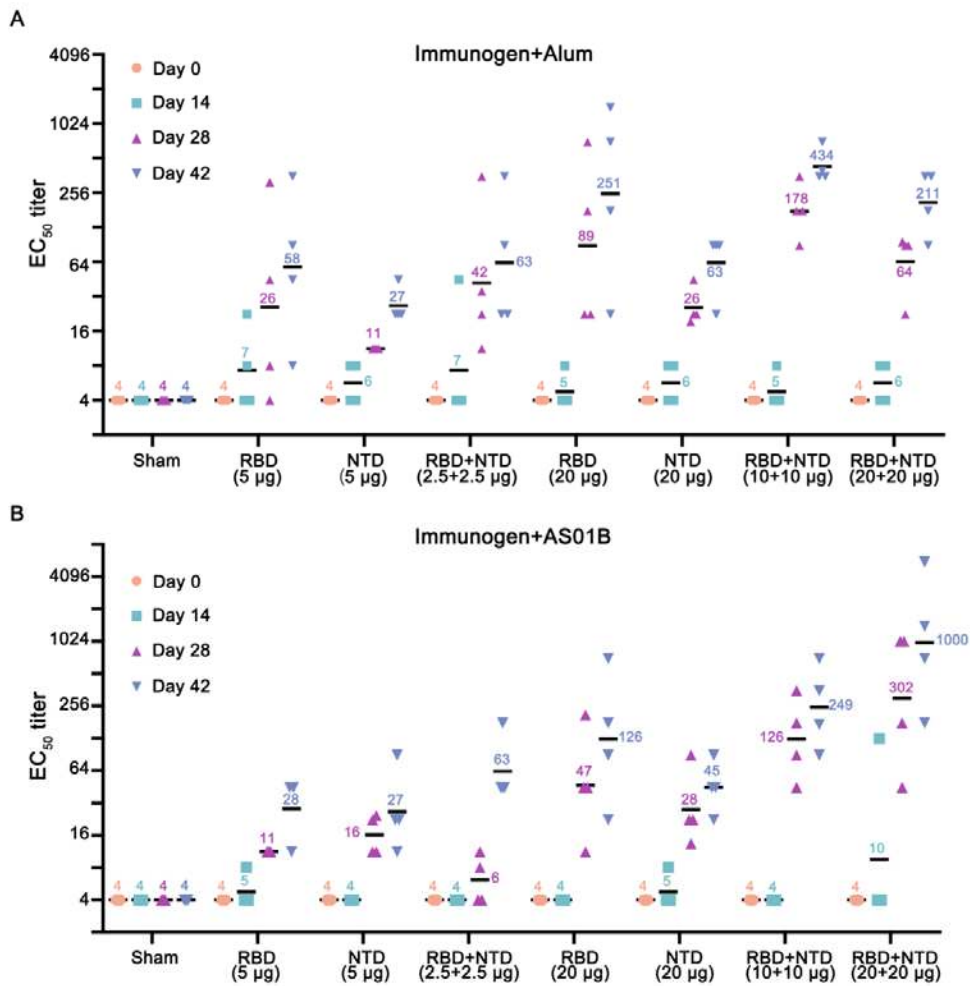
481

482

483

484

485



487 **Figure 4. Immunogenic evaluation of candidate antigen formulations mixed with alum or**
488 **AS01B adjuvant in rabbits.** (A-B) Rabbits were immunized intramuscularly with various doses
489 of individual (RBD or NTD) or combined (RBD+NTD) immunogens mixed with alum or AS01B
490 adjuvant or adjuvant only (sham) (n=4). Neutralizing antibody titer against live SARS-CoV-2 was
491 measured. Data points represent mean +/- SEM of individual rabbits from four independent
492 experiments; error bars reflect SEM; horizontal lines indicate the geometric mean titer (GMT) of
493 EC₅₀ for each group.

494

495

496

497